In Situ Observations of the Formation of Periodic Collisionless Plasma Shocks from Fast Mode Waves

Lican Shan, Aimin D Du, Bruce T Tsurutani, Yasong Ge, Quanming Lu, Christian Mazelle, Can Huang, Karl-Heinz Glassmeier, Pierre Henri

▶ **To cite this version:**

Lican Shan, Aimin D Du, Bruce T Tsurutani, Yasong Ge, Quanming Lu, et al.. In Situ Observations of the Formation of Periodic Collisionless Plasma Shocks from Fast Mode Waves. The Astrophysical journal letters, 2020, 888 (2), pp.L17. 10.3847/2041-8213/ab5db3 . insu-02514825

HAL Id: insu-02514825
https://insu.hal.science/insu-02514825

Submitted on 18 May 2020

HAL is a multi-disciplinary open access archive for the deposit and dissemination of scientific research documents, whether they are published or not. The documents may come from teaching and research institutions in France or abroad, or from public or private research centers.

L'archive ouverte pluridisciplinaire **HAL**, est destinée au dépôt et à la diffusion de documents scientifiques de niveau recherche, publiés ou non, émanant des établissements d'enseignement et de recherche français ou étrangers, des laboratoires publics ou privés.

The Astrophysical Journal Letters, 888:L17 (5pp), 2020 January 10 https://doi.org/10.3847/2041-8213/ab5db3
© 2020 The Author(s). Published by the American Astronomical Society.

In Situ Observations of the Formation of Periodic Collisionless Plasma Shocks from Fast Mode Waves

Lican Shan[1,2,10], Aimin Du[1,2,3,10], Bruce T. Tsurutani[4], Yasong S. Ge[1,2,3], Quanming Lu[5,6], Christian Mazelle[7], Can Huang[1,2], Karl-Heinz Glassmeier[8], and Pierre Henri[9]

[1] Key Laboratory of Earth and Planetary Physics, Institute of Geology and Geophysics, Chinese Academy of Sciences, Beijing, 100029, People's Republic of China
ysge@mail.iggcas.ac.cn
[2] Innovation Academy for Earth Science, CAS, Beijing, 100029, People's Republic of China
[3] College of Earth and Planetary Sciences, University of Chinese Academy of Sciences, Beijing, 100049, People's Republic of China
[4] Independent Scholar, Pasadena, California, 91109, USA
[5] CAS Key Lab of Geospace Environment, University of Science and Technology of China, Hefei, 230026, People's Republic of China
[6] CAS Center for Excellence in Comparative Planetology, People's Republic of China
[7] Institut de Recherche en Astrophysique et Planétologie, University Paul Sabatier, CNRS, Toulouse, F-31400, France
[8] Institut für Geophysik und extraterrestrische Physik, Technische Universität Braunschweig, Mendelssohnstrae 3, D-38116, Braunschweig, Germany
[9] Laboratoire de Physique et Chimie de l'Environnement et de l'Espace, UMR 7328 CNRS, Université d'Orléans, F-45100, Orléans, France
Received 2019 November 20; accepted 2019 November 27; published 2020 January 9

Abstract

It has been long theorized, but not directly observed, that low-frequency magnetosonic plasma waves can steepen and form shocks. We show an example of small-amplitude, sinusoidal magnetosonic waves at the proton gyrofrequency upstream of the Martian bow shock. We hypothesize that these waves are produced by an ion beam instability associated with the ionization of hydrogen atoms by charge exchange with solar wind protons, solar photoionization, and/or electron impact ionization. As the waves are convected toward the planet by solar wind flow, the wave amplitude grows due to additional free energy put into the system by further ion beam particles. Finally, the steepened waves form shocks. Because of their development, the shocks are periodic with the separation at the proton gyroperiod. These observations lead to the conclusion that newborn ions may play a crucial role in the formation process of some collisionless plasma shocks in astrophysical and space plasmas.

Unified Astronomy Thesaurus concepts: Shocks (2086); Pickup ions (1239); Plasma physics (2089)

1. Introduction

Collisionless plasma shocks (CPSs) are believed to be abundant in astrophysical plasmas. They occur when a super-magnetosonic streaming plasma encounters a blunt obstacle with a magnetic field, a planetary or cometary ionosphere, or a slowly moving or stagnant plasma. CPSs are responsible for the acceleration of energetic (~TeV) cosmic rays (Aharonian et al. 2004) and solar flare energetic particles (Tsurutani & Lin 1985; Reames 1999; Turner et al. 2018). Nevertheless, how CPSs form in the vast universe is still one of the biggest mysteries in astrophysics. Presently, one well-accepted theory is that small-amplitude, low-frequency sinusoidal waves are excited by a backstreaming ion beam through a background plasma (Kennel & Petschek 1966). As the instability continues to grow, the amplitudes of the sinusoidal waves increase. Nonlinear forces and the addition of more free energy input cause the waves to steepen (Treumann 2009). In view of magnetohydrodynamics theory, when further steepening occurs, the waves will ultimately break until the shock dissipation and dispersion happen, which limits or balances the nonlinear process (Haerendel & Paschmann 1982; Kennel et al. 1985; Treumann & Baumjohann 1997). These waves evolve into phase-steepened, large-amplitude waves, and finally to CPSs that are both dispersive and dissipative. However, in situ measurements of CPSs that have evolved from linear waves have not yet been observed.

2. Observations

In this Letter, we report in situ observations of an entire formation sequence of the periodic plasma shocks by the *Mars Atmosphere and Volatile Evolution* (*MAVEN*) instrumentation, as the spacecraft travels through the solar wind, the Martian exosphere, and ionosphere (see Figure 1). The developed shocks are intriguing because their original waves are excited by newborn ions when we analyze the wave properties. The newborn ions are created by photoionization, charge exchange, and electron impact ionization (Rahmati et al. 2017) of the escaped neutral atoms of the Martian exosphere. The newly formed ions are an ion beam in the solar wind plasma frame and become the source of plasma instabilities for the sinusoidal seed electromagnetic waves, and ultimately for the shocks. This provides the possibility of studying the shock formation process behind some astrophysical and space plasma scenarios.

The full view of the various stages of sinusoidal wave evolution during this event on 2015 February 12 are demonstrated by the magnetic field variations in four time intervals marked by different color bars in Figure 2(a): quasi-sinusoidal low-frequency waves (QSLFWs), nonsinusoidal phase-steepened waves (NPSWs), fast mode periodic shocks (FMPSs), and magnetosonic collisionless shocks (MCSs). Individual stage of the wave evolution have been observed at Mars (Dubinin & Fraenz 2016; Collinson et al. 2018; Halekas et al. 2019). The interplanetary magnetic field (Figure 2(a)) is measured by the Magnetometer (MAG) instrument (Connerney et al. 2015). We calculated the average field with a low-pass filter from 0 to 0.04 Hz during the interval from 01:25 to 01:32 UT. The average field has a small inclination ($\theta_{Bx} \sim 34°$) from the x-axis of Mars Solar Orbital (MSO) coordinates and a constant magnitude. Within this quiet solar wind, we identify an interval of the QSLFW with the average magnetic magnitude of $\sim 3.03 \pm 0.34$ nT (Figure 2(b)). The frequency of the observed waves (0.041 Hz) is very close the local proton gyrofrequency

[10] These authors contributed equally to this work.

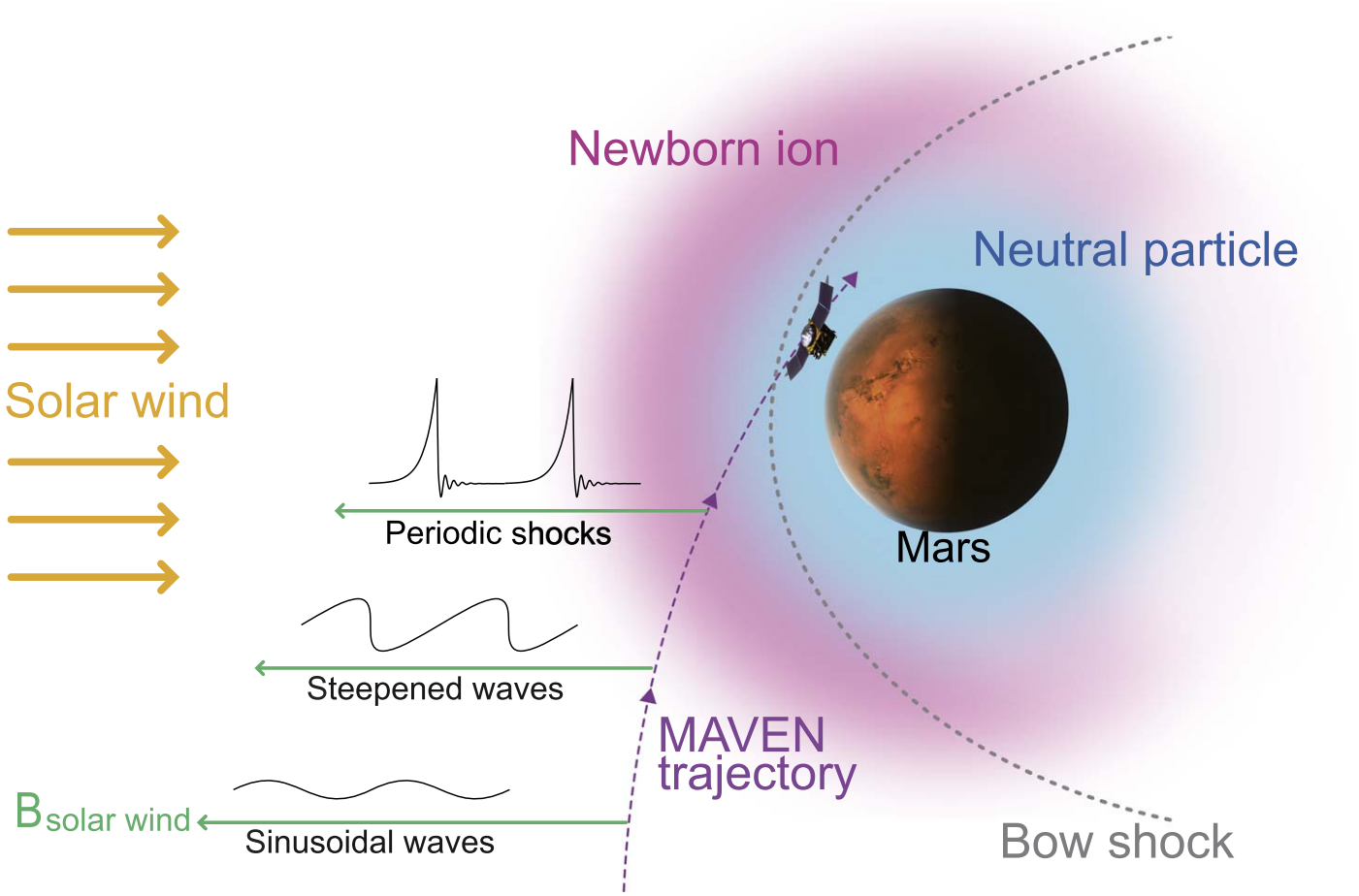

Figure 1. Sketch of observations for wave evolution at Mars. The *MAVEN* spacecraft was moving from the solar wind to the ionosphere. Along the spacecraft trajectory, waves and their evolution were observed. The purple dashed line represents the *MAVEN* trajectory. The black curves are typical waveforms during the evolution, which are idealizations of the magnetic signals B_z shown in Figure 3. For simplicity and illustration, we have drawn the magnetic field as radial. A hydrogen exosphere including neutral particles and newborn protons extends beyond the Martian ionosphere (Galli et al. 2006). An expected bow shock made by a model (Vignes et al. 2000) is represented by a gray dashed curve.

(black lines in Figures 2(d) and (e)). Considering that the newborn ions are at rest in the spacecraft frame but move at a speed of v_{sw} ($\sim$350 km s^{-1} for this case) relative to the solar wind plasma (Tsurutani & Smith 1986), the wave frequency (ω) in the plasma rest frame satisfies the resonant condition: $\boldsymbol{\omega} - \boldsymbol{k} \cdot \boldsymbol{v} = -n\boldsymbol{\Omega}_i$, where $\boldsymbol{k}$ is the wave vector, $\boldsymbol{v}$ is the ion velocity, n is an integer (in this case equal to one), and $\boldsymbol{\Omega}_i$ ($=qB/m$, q, and m are the charge and mass of the ion) is the local ion gyrofrequency. Those waves propagate almost parallel to the Mars–Sun line at an angle of $\theta_{kB} \sim 19°$ relative to the ambient magnetic direction, and $\theta_{kx} \sim 33°$ relative to the x-axis. As the sinusoidal waves are convected by the solar wind closer to Mars, the wave field components start to steepen at the same edge, and the wave amplitudes increase to $\sim$5 nT. This is the NPSW stage of development. From $\sim$01:37 UT, the sunward ion flux measured by the SupraThermal And Thermal Ion Composition instrument (STATIC; McFadden et al. 2015) are enhanced (Figure 2(f)), which drive the NPSWs to further steepen and intensify. The sunward proton flux increases from $\sim 2.19 \times 10^5$ to 1.15×10^6 eV cm^{-2} s^{-1} sr^{-1} eV^{-1} during the interval from $\sim$01:34 to 01:46 UT in the solar wind. The steepening process increases the wave amplitudes up to $\sim$10 nT, and finally forms the FMPSs that have a similar period to the QSLFW. The dominant wave frequency during the first three stages is $\sim$0.041 Hz (the local proton gyrofrequency is $\sim$0.045 Hz) until strong compression appears at about 01:47 UT. This indicates that the spatial separation between two adjacent shocks is essentially determined by the newborn ion gyromotion. The low-frequency magnetic field variations from the compression merge with FMPSs to form MCS, which enlarges wave amplitude up to $\sim$20 nT. The shock angle (between shock normal and the ambient magnetic field) and compression ratio for MCSs are $\sim$66° and $\sim$2.7, respectively. The magnetosonic Mach number of MCSs is $\sim$4.2, which is calculated with the data from the Solar Wind Electron Analyzer (SWEA; Mitchell et al. 2016) and the Solar Wind Ion Analyzer (SWIA; Halekas et al. 2015) instruments.

High-resolution (32 Hz) magnetic field data record the evolution of the waveforms and the polarizations of the waves during periodic shock development. The magnetic field components of the QSLFW vary in similar quasi-sinusoidal waveforms with a fixed phase difference (Figure 3(a)). Then as the waves are growing in amplitude, nonlinear processes lead to the evolution of the sinusoidal waves into phase-steepened waves. The magnetic field variations transfer into the beach-wave-like waveforms during the steepening process (NPSW; Figure 3(b)). As almost all of the wave phase rotation occurred in a fraction of the original wavelength, the wave fronts further steepen and eventually develop into periodic shocks (FMPS; Figure 3(c)). The QSLFWs, generated by an ion beam instability (Wu & Davidson 1972), are right-hand circularly polarized in

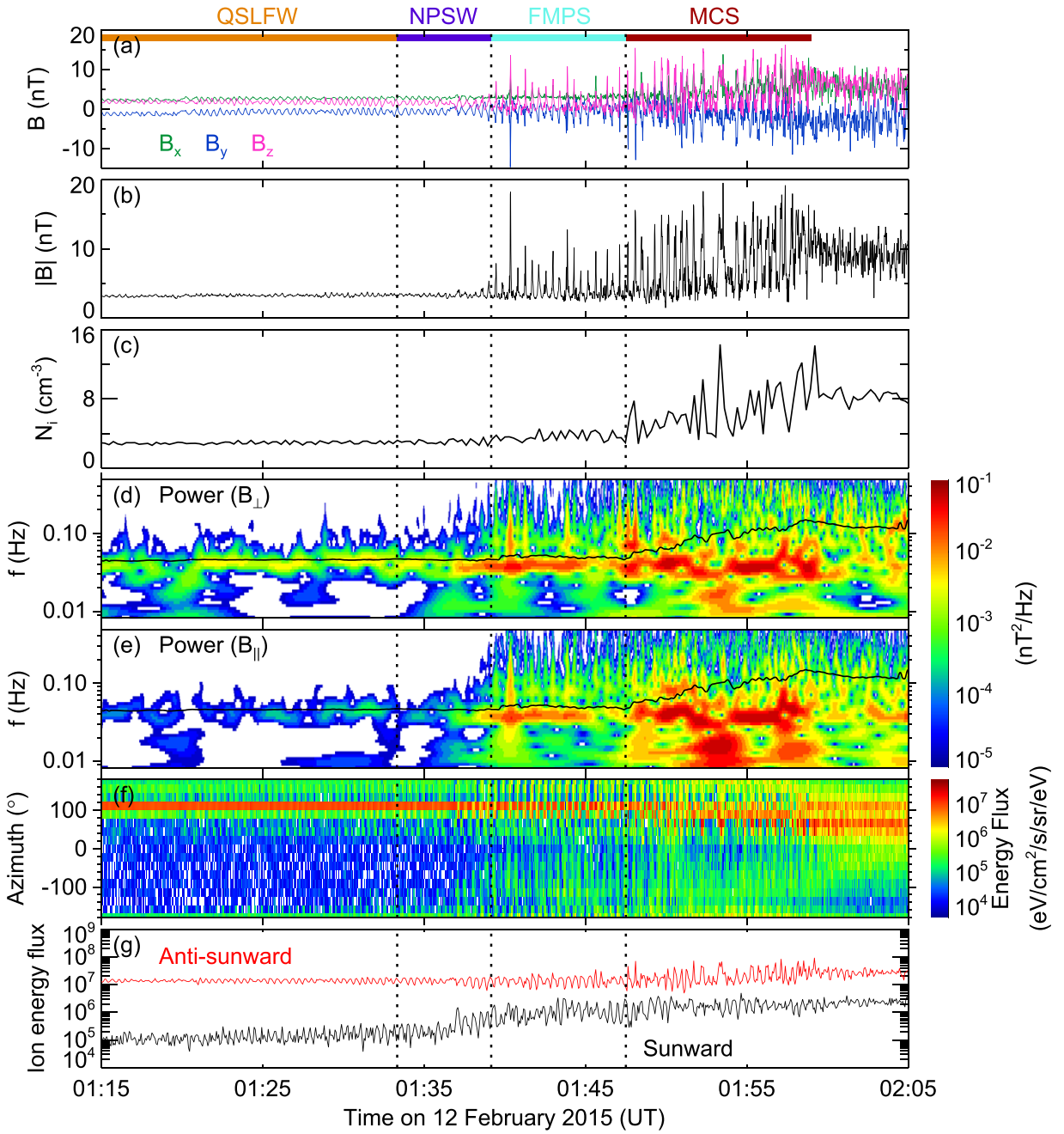

Figure 2. Time series for wave evolution on 2015 February 12. (a) and (b) 1 Hz sampled magnetic field and magnitude from MAG. The different intervals of wave development are labeled QSLFW, NPSW, FMPS, and MCS to illustrate the different stages of the wave evolution, which are marked by orange, purple, cyan, and crimson bars, respectively. (c) Ion number density from STATIC D1 data. For this event, STATIC provides a 360° (azimuth) × 90° (elevation) field of view, which measured both solar wind and planetary ions. (d) and (e) Power spectrum of magnetic field for perpendicular and parallel directions. Here the perpendicular direction is along the ambient $\boldsymbol{B_o} \times \boldsymbol{x}$-MSO. For MSO coordinates, and the x direction is along the Mars–Sun line; y is directed opposite to the orbital velocity of Mars, and z completes the right-handed coordinate system. The local proton gyrofrequency is marked by black lines and its average is ∼0.045 ± 0.005 Hz during the QSLFW interval. (f) Ion energy fluxes (STATIC CA data) for different azimuth in the STATIC frame. Solar wind ions have an azimuth angle ∼110°. From ∼01:37, increasingly sunward protons were measured at an average azimuth ∼−100°, which is about 150° from the solar wind direction. (g) Anti-sunward (red) and sunward (black) ion energy fluxes. We sum the fluxes in the angle range [−168.°75, 11.°25] for sunward, [−180°, −168.°75] and [11.°25, 180°] for anti-sunward fluxes.

the plasma frame. Because of the anomalous Doppler shift of the solar wind convecting the waves past the spacecraft (Tsurutani 1991; Tsurutani et al. 1995), they exhibit a left-hand circular polarization with respect to the background magnetic field in the spacecraft frame (Figure 3(d)) and have a frequency at local proton gyrofrequency. As the waves develop and the amplitudes increase at wave fronts, they become slightly elliptically polarized at the stage of NPSW (Figure 3(e)). Then later, even linearly polarizations are detected at the FMPS stage (Figure 3(f)) but with the same period. High-frequency (average ∼1.3 s) dispersive whistler waves were also observed and usually associated with these FMPSs, which has been previously investigated associated with shock and shocklet structures (Sagdeev 1966; Hoppe & Russell 1980; Mellott 1985; Tsurutani et al. 1989; Sundkvist et al. 2012). These dispersive whistlers are one form of balance to the shock nonlinearity features (Haerendel & Paschmann 1982; Kennel et al. 1985; Treumann & Baumjohann 1997; Sundkvist et al. 2012).

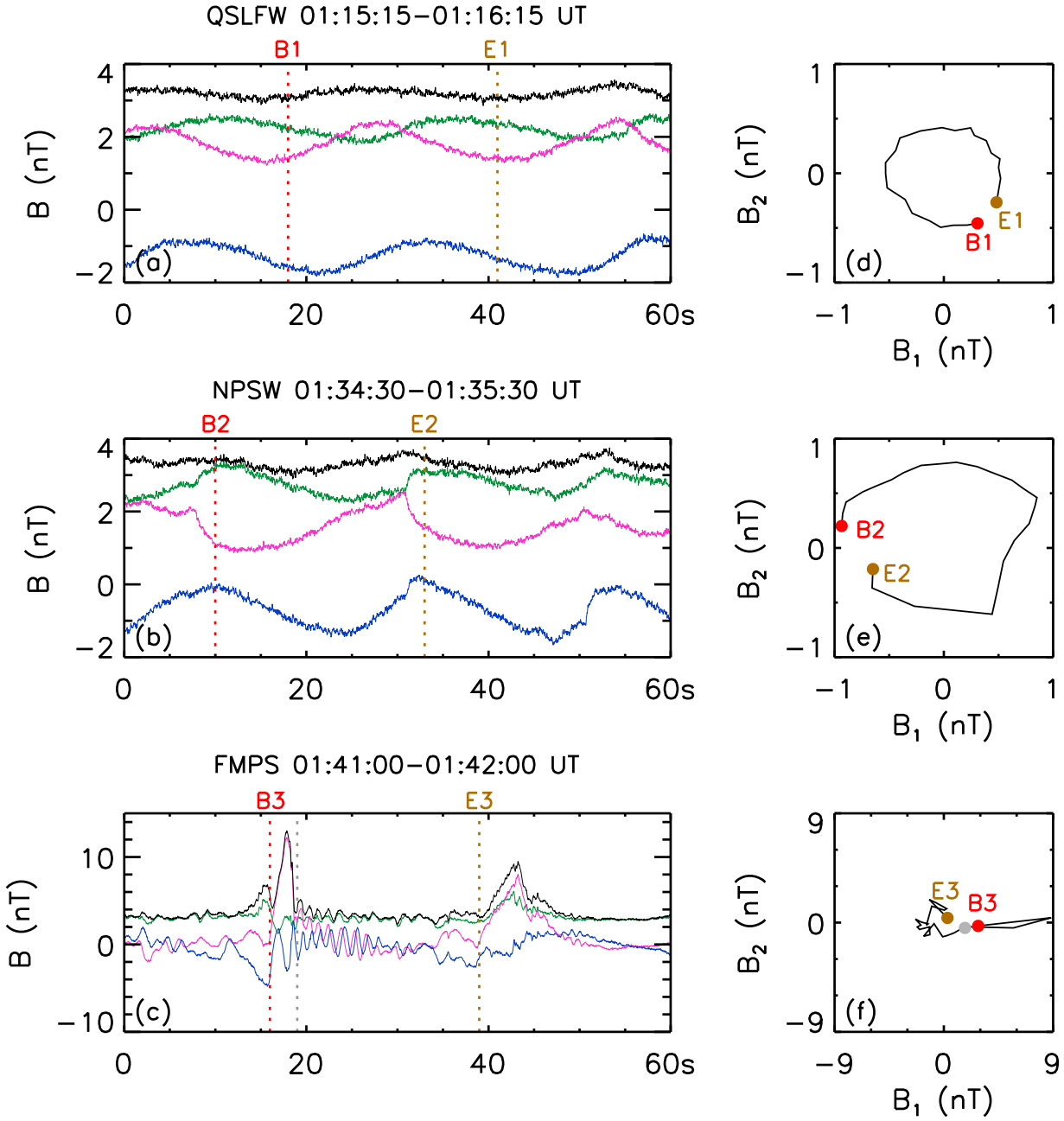

Figure 3. Examples of the stages of wave evolution. (a)–(c) 32 Hz sample of 60 s magnetic field data show the QSLFW, NPSW, and FMPS stages during the wave evolution process. Green, blue, pink, and black lines show the B_x, B_y, B_z and the magnetic magnitude, respectively. (d)–(f) hodogram analysis of 1 Hz magnetic field data for about one single cycle of QSLFW, NPSW, and FMPS, respectively. B_1 and B_2 are the magnetic field components in the wave plane, which is perpendicular to the wave propagation direction. In the B_1–B_2 plane, the ambient magnetic field points out the plane. B (red) and E (brown) mark the beginning and end of the interval, respectively. The wave exhibits a left-handed polarization with respect to background field in the spacecraft frame. In QSLFW, the wave period is ∼25 s, which is essentially the local proton cycle (∼22 s). The spatial separation between the adjacent periodic shocks depends on the newborn proton cyclotron motion.

3. Conclusions and Discussion

From in situ observations we show the evolution from sinusoidal fast magnetosonic waves to periodic plasma shocks. The sinusoidal waves are excited by a beam of newborn ions in the solar wind. In the particular situation where the interplanetary magnetic field is parallel to the solar wind velocity direction, right-hand magnetosonic waves are generated, with the maximum growth rate, by the ion beam instability. Once the sinusoidal magnetosonic waves have been generated, they phase-steepen so that all of the circular phase rotation is condensed at the steepened edge. Meanwhile, the wave amplitude at the steepened edge grows due to the nonlinear steepening process and the addition of fresh free energy from the addition of new ions to the beam. During the interval from 2014 October to 2017 February, we identified 158 events with steepening waves/periodic shocks. This event is the best clear one that shows the entire formation sequence of the wave evolution. In this event, the fast mode waves take about one minute to steepen when there is sufficient beam energy input. Moreover, we find that most (∼62.6%) of the steepened waves are observed under the condition of small interplanetary magnetic field inclinations ($\theta_{Bx} < 40°$). This type of large-amplitude nonlinear magnetosonic waves associated with

pickup ions were also previously detected in cometary plasmas (Tsurutani & Smith 1986; Glassmeier & Neubauer 1993; Mazelle et al. 1995). The steepening process of magnetosonic waves has been conducted by numerical simulations in two stages (Omidi & Winske 1990). With further steepening and additional free energy, the nonlinear waves evolve into periodic shocks. The similar signals of electron density were also identified at comet Grigg-skjellerup (Rème et al. 1993), illustrating the possibility that the same formation mechanism exists for such periodic shocks. Due to the lack of a global intrinsic magnetic field, the Martian bow shock is close to the planet (subsolar distance from the planet center is ~5600 km; Vignes et al. 2000), and the Martian exosphere extends beyond the bow shock. The ion pickup process occurs because these neutrals exist in the pure solar wind. At the Earth, the magnetosphere extends to $\sim 10\,R_E$ (radius of Earth) in the sunward direction and the bow shock is another $\sim 3\,R_E$ further away. Thus there are very few neutral particles upstream of the Earth's bow shock.

The above description of plasma wave evolution into periodic shocks is simply an interpretation of spacecraft observations. These results extend the current knowledge of the CPS formation, especially in the astrophysical environment with newborn ions. However, the microphysical process, the interactions of newborn ions with steepened waves, and the periodic shocks that would control the shock formation, remain to be understood. Theoretical and simulated research is needed to resolve these issues. We expect that this will become a new exciting area of CPS studies.

We are indebted to the *MAVEN* team for the design and successful operation of the mission. The *MAVEN* data are publicly available through the Planetary Data System (https://pds-ppi.igpp.ucla.edu). We wish to thank J. McFadden, J. Espley, D. Mitchell, J. Halekas, and B. Jakosky for discussions about the data. L.S. thanks T.Z. Liu and Z. Yang for discussions, and E. Penou for his assistance in data processing. This work is supported by the National Key Research and Development Program of China (2016YFB0501300, 2016YFB0501304), the National Natural Science Foundation of China (grant Nos. 41774187, 41674168, 41774176), Beijing Municipal Science and Technology Commission (grant No. Z191100004319001), the Strategic Priority Research Program of Chinese Academy of Sciences (grant No. XDA14040404), and the pre-research Project on Civil Aerospace Technologies No. D020103 funded by CNSA.

ORCID iDs

Lican Shan https://orcid.org/0000-0002-2354-9261
Quanming Lu https://orcid.org/0000-0003-3041-2682

References

Aharonian, F. A., Akhperjanian, A. G., Ave, K.-M., et al. 2004, Natur, 432, 75
Collinson, G., Wilson, L. B., Omidi, N., et al. 2018, JGRA, 123, 7241
Connerney, J. E. P., Esple, J., Lawton, P., et al. 2015, SSRv, 195, 257
Dubinin, E., & Fraenz, M. 2016, GMS, 261, 343
Galli, A., Wurz, P., Lammer, H., et al. 2006, The Mars Plasma Environment (Dordrecht: Springer)
Glassmeier, K.-H., & Neubauer, F. M. 1993, JGR, 98, 20921
Haerendel, G., & Paschmann, G. A. 1982, Magnetospheric Plasma Physics (Tokyo: Center for Academic Publications Japan)
Halekas, J. S., Luhmann, J. G., Dubinin, E., & Ma, Y. 2019, JGR, in press
Halekas, J. S., Taylor, E. R., Dalton, G., et al. 2015, SSRv, 195, 125
Hoppe, M., & Russell, C. T. 1980, Natur, 287, 417
Kennel, C. F., Edmiston, J. P., & Hada, T. 1985, GMS, 34, 1
Kennel, C. F., & Petschek, H. E. 1966, JGR, 71, 1
Mazelle, C., Rème, H., Neubauer, F. M., & Glassmeier, K.-H. 1995, AdSpR, 16, 41
McFadden, J. P., Kortmann, O., Curtis, D., et al. 2015, SSRv, 195, 199
Mellott, M. M. 1985, GMS, 35, 131
Mitchell, D. L., Mazelle, C., Sauvaud, J.-A., et al. 2016, SSRv, 200, 495
Omidi, N., & Winske, D. 1990, JGR, 95, 2281
Rahmati, A., Larson, D. E., Cravens, T. E., et al. 2017, JGRA, 122, 3689
Reames, D. V. 1999, SSRv, 90, 413
Rème, H., Mazelle, C., Sauvaud, J. A., et al. 1993, JGR, 98, 20965
Sagdeev, R. Z. 1966, RvPP, 4, 23
Sundkvist, D., Krasnoselskikh, V., Bale, S. D., et al. 2012, PhRvL, 108, 025002
Treumann, R. A. 2009, A&ARv, 17, 409
Treumann, R. A., & Baumjohann, W. 1997, Advanced Space Plasma Physics (London: Imperial College Press)
Tsurutani, B. T. 1991, GMS, 61, 189
Tsurutani, B. T., Glassmeier, K.-H., & Neubauer, F. M. 1995, GeoRL, 22, 1149
Tsurutani, B. T., & Lin, R. P. 1985, JGR, 90, 1
Tsurutani, B. T., & Smith, E. L. 1986, GeoRL, 13, 263
Tsurutani, B. T., Smith, E. J., Brinca, A. L., Thorne, R. M., & Matsumoto, H. 1989, P&SS, 37, 167
Turner, D. L., Wilson, L. B., Liu, T. Z., et al. 2018, Natur, 561, 206
Vignes, D., Mazelle, C., Rème, H., et al. 2000, GeoRL, 27, 49
Wu, C. S., & Davidson, R. C. 1972, JGR, 77, 5399